JAAS

Journal of Analytical Atomic Spectrometry

www.rsc.org/jaas

Volume 28 | Number 6 | June 2013 | Pages 771–960

ISSN 0267-9477

RSC Publishing

PAPER

J. J. Laserna *et al.*

Evaluating the use of standoff LIBS in architectural heritage: surveying the Cathedral of Málaga

0267-9477(2013)28:6;1-0

JAAS

RSC Publishing

PAPER

View Article Online
View Journal | View Issue

Cite this: *J. Anal. At. Spectrom.*, 2013, **28**, 810

Evaluating the use of standoff LIBS in architectural heritage: surveying the Cathedral of Málaga

I. Gaona, P. Lucena, J. Moros, F. J. Fortes, S. Guirado, J. Serrano and J. J. Laserna*

Laser-induced breakdown spectroscopy (LIBS) is a cutting-edge technology which offers appealing features for its application in the field of the cultural heritage. It is a proven technology for the fast and simultaneous detection of major and trace elements with minimal destructiveness, using easily compactable instrumentation into movable platforms for the *in situ* and standoff chemical analysis of objects in real time. In the present work, a standoff LIBS sensor has been used for surveying the Cathedral of Málaga. The spectroscopic measurements were gathered *in situ* although from an averaged distance of 35 m. A comprehensive characterization of the materials composing the main façade as well as identification of the noticeable pollutants at their surfaces has been performed. The standoff LIBS results have fitted neatly with the mineralogical analysis of all the stones assayed. The large emissions of Si, Al, Ca and Mg have confirmed that the structure was almost entirely built using sandstone. In turn, the sensitivity to carbonate chemistry has demonstrated the capability of standoff LIBS for coherently classifying different marbles, thus allowing the identification of their origins. Standoff LIBS has also allowed the detection of pollutants such as Si, Ca, Mg, Fe, Al, Ba and Sr, originating from natural sources such as the transport of re-suspended dust and atmospheric particulate matter related to marine aerosols. In addition, trace elements such as Ti, Pb and Mn from exhausts of gasoline and diesel engines are also involved in the pollution triggering of materials. To obtain all these findings, scaffolding or other intrusive facilities have not been required.

Received 1st March 2013
Accepted 18th April 2013

DOI: 10.1039/c3ja50069a

www.rsc.org/jaas

1 Introduction

Cultural heritage is a valuable resource inherited from the history and a unique legacy that broadens our understanding of the diversity of society and its constant evolution. Whether they are objects or archaeological sites, or ancient and historic monuments of the world, all of them inform and help connect us to our cultural origins. Therefore it is a real and irreplaceable treasure of outstanding value, considered worthy of preservation. Unfortunately, the rapid and on-going evolution of society has brought about a large deterioration of these vast sources of culture. Effects not only from anthropogenic sources but also from natural causes can result in unlimited and irreversible damage in cultural heritage. All this has meant that the conservation of cultural heritage and its protection against possible damage due to pollution has received growing scientific interest. In order to find the best possible measures for proceeding with protection of cultural heritage material, provision of analytical information for its characterization is a vital requirement. Further, research efforts to better assess and understand the pollution sources and mechanisms damaging the cultural heritage material cannot be set aside. Strong evidence of the growing importance of these physical and chemical diagnostics is the wide aim of analytical techniques used for this end.[1,2]

Scientific assessment of the materials for cultural heritage poses specific, and often, difficult analytical challenges. The primary requirement is that no significant modification or alteration of the artifact occurs, so as not to compromise the historical, cultural and/or archaeological value when extracting as much information as possible.[3] Also, the capability of working *in situ* and in real time, either during the research campaigns[4,5] or after the consequent conservation tasks,[6] is often necessary due to the impossibility of moving historical artifacts to laboratory facilities. The use of compact, robust, and versatile analytical systems is highly desirable.[7] Finally, the limited or complex accessibility to the assets is often incompatible with conventional methods of analysis. This circumstance requires the use of instruments to operate in a contactless way, but rapidly and with appropriate sensitivity.[8]

Although few analytical techniques pool all these demands, laser-induced breakdown spectroscopy (LIBS) is an appealing tool for analysis that combines the above requirements.[9,10] LIBS is a established technology having several advantages over conventional elemental analysis methods. Its capacity for rapidly and simultaneously detecting almost all elements after the ablation of barely a few nanograms of a target analyzed from

Department of Analytical Chemistry, Faculty of Sciences, University of Málaga, E29071 Málaga, Spain. E-mail: laserna@uma.es; Fax: +34 95 213 2000; Tel: +34 95 213 1881

several tens of meters from the portable platform is now a reality.[11] The potential of LIBS in the analysis of works of art and objects of archaeological importance has been demonstrated by several research papers that have appeared in the last few years.[12] They describe its use in the major and trace element analysis of paintings,[13] frescoes,[14] pottery,[15,16] marbles,[17] alloys[18] and ancient stones,[19] among others, for dating and characterizing provenance.[20] Furthermore, LIBS has also been used to diagnose contamination[21,22] of heritage assets and as a tool either to deal with cleaning tasks or for their diagnosis.[23,24] The versatility of connecting LIBS with other laser analytical techniques, such as laser-induced fluorescence (LIF) spectroscopy,[25] Raman microscopy,[26–28] X-ray fluorescence (XRF),[29] as well as its capability of operating underwater[30] makes LIBS a cutting-edge technique to be used.

Up to date, only fluorescence LIDAR (LIght Detection And Ranging) has been able to address the remote, non-invasive diagnostics of cultural heritage stone in the outdoor environment.[31] Early experiments on monuments date back to the mid 1990s, when fluorescence LIDAR point measurements were conducted on the Cathedral and Baptistery of Parma, Italy.[32] Experiments dealing with the remote monitoring of biodeteriogens on stone surfaces[33] (important cause of the weathering of a monument) and the characterization of different types of stones of the building materials[34] were performed. Subsequently, the technique has taken further advantage of the introduction of imaging capabilities in LIDAR instrumentation, thereby allowing the acquisition of hyperspectral fluorescence maps from an extended area at distances as large as 65 m, as for example for the documentation of past conservation interventions on the Colosseum, Rome.[35] However, despite this technique's ability to supply valuable analytical information, its main disadvantage arise from its 'one wavelength–one transition' selectivity which prevents it from getting the entire atomic information that LIBS gathers.

In this work, the potential of LIBS technology to obtain multielemental information about materials and their contamination from the analysis *in situ* but from away (35 meters) has been demonstrated for the first time from a case study on one of the most important Renaissance architectural jewels in Andalusia, the Cathedral of Málaga. A thorough characterization of the sandstones, marbles and metals making up the most highlighted section of the main façade of this historical building has been performed. In turn, the identification of the most relevant pollutants that are damaging its appearance has also been accomplished.

2 Experimental

2.1 Standoff LIBS sensor

The standoff LIBS sensor uses a high power double-pulse Nd:YAG laser system (Brilliant Twins, @ 1064 nm, 10 Hz, 850 mJ per pulse, 5.5 ns pulse width) as the excitation source. Both delivered laser beams are perfectly spatially overlapped, but with a temporal delay (600 ns) inherent to the electronics. The laser beam is guided towards its output by consecutive reflections on five laser mirrors of an articulated arm (Applied Photonics Ltd.). At the exit of the optical arm, a dichroic mirror (at a 45° angle) reflects the beam towards a 400 mm aperture classical Cassegrain open-truss telescope (Optical Guidance Systems) used to focus the beam onto the distant target. The expanded beam, which enters into the telescope through a back aperture, is first directed to a secondary mirror and then reflected towards a primary mirror, which finally focuses it at the desired target. With a motorized mirror shift mechanism, the working distance may be adequately adjusted. The telescope is mounted on an altitude-azimuth fork, thus enabling the inspection of well-defined areas. The accuracy on the pointing of the excitation beam upon the distant targets is obtained with the help of a diode laser (635 nm). Bearing in mind the maximum focus of the laser beam (*ca.* 3 mm in diameter at 30 m distance) as measured in the lab facilities, theoretical irradiance values at the real scenario are expected to span from 0.8 GW cm^{-2} up to *ca.* 2 GW cm^{-2}. The laser damage of materials is a complex outcome not only from the energy density of the laser beam but also from the number of laser shots and the nature of the sample analyzed. Thus, an assessment of the damage caused by the beam at the irradiance used was also made at the lab facilities. In all cases, the damage caused by the LIBS inspection in the surface finish of the materials after 1000 laser shots was entirely negligible.

Once produced, plasma light is also collected by the telescope, first directed through an aperture in the primary mirror and then reflected towards the secondary mirror, which finally focuses it behind the dichroic mirror. The plasma image is guided to a spectrometer (Andor SR-303i) using a 2 m long, 600 μm diameter optical fiber. The spectrometer is fitted with a 1200 grooves mm^{-1}, 300 nm blazed grating, providing a spectral window that ranges from 370 nm to 440 nm. Dispersed light is registered using an intensified charge coupled device – iCCD – (Andor iStar DH740-25F-03). The timing parameters used for spectral acquisition are: 2 μs as the delay time from the input of an external trigger (considered as zero time) to the opening of the intensifier tube of the detector device, and 5 μs as the integration time. More details may read in ref. 36.

2.2 Scenario description

The Cathedral of Málaga is a noteworthy piece of Renaissance architecture in Spain. This historical monument was constructed between 1528 and 1782. The façade is divided into three well-defined areas, separated by Corinthian columns. In the present work, the central wing of the lower level was studied. The analysis of the medallion therein located, and those ornamental elements that flank it, was the focus of our investigations. Fig. 1 shows a model of the Cathedral locating the working scenario. The sensor emplacement and a detailed image of the tested area are also highlighted. A thorough *in situ* standoff LIBS survey to characterize the composition of the materials and to detect potential pollutants spoiling the appearance of the most significant ornate stoneworks within this area was performed. The most adequate sampling strategy that best reflected what was essential to each evaluation was established. Thus, within each spectral series, while early laser events were considered for the detection of pollutants, the characterization of materials was made from the latter laser events.

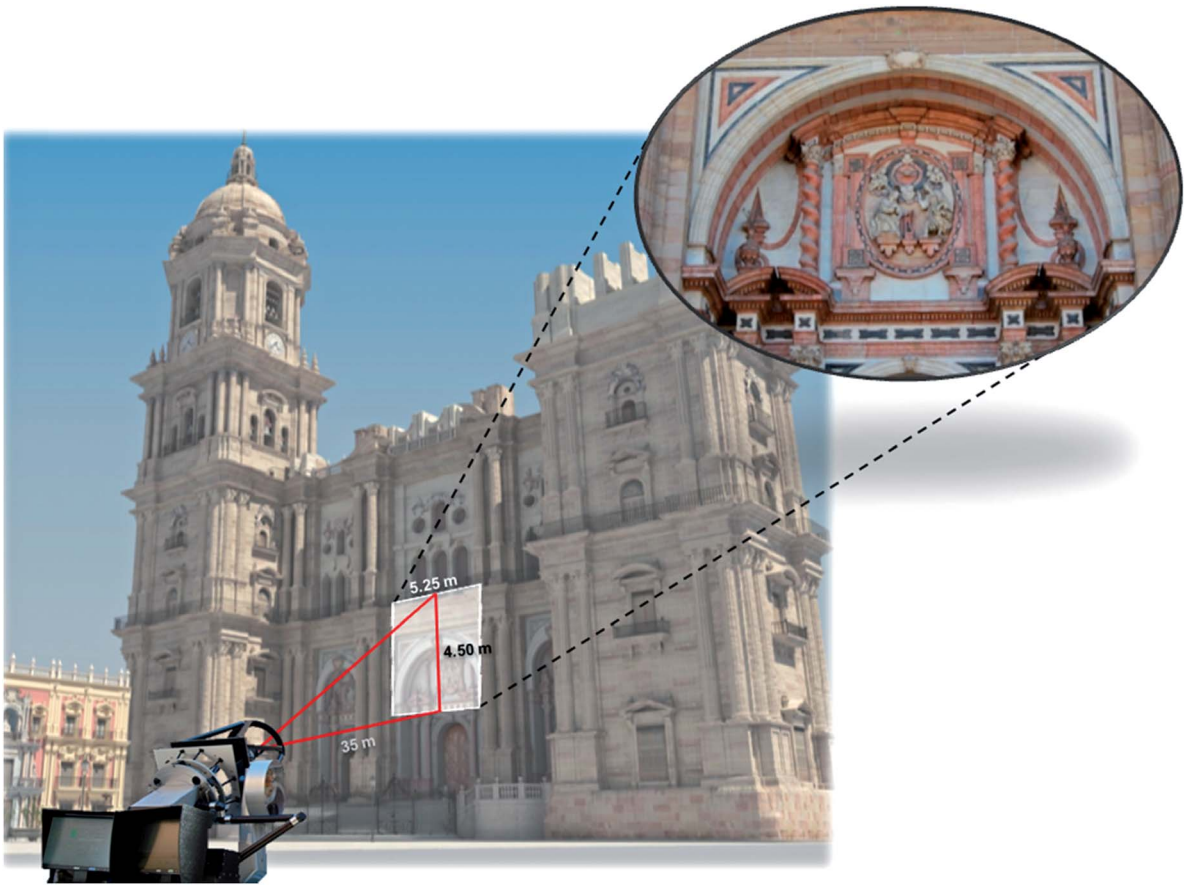

Fig. 1 Descriptive scheme on the working scenario. The emplacement of the LIBS platform, and section investigated, are highlighted.

3 Results and discussion

3.1 Multielemental profiling

With the aim of identifying the chemical composition of the materials forming part of the architectural objects within the investigated section of the Cathedral's main façade, a broad deployment of surface laser interrogations was carried out. The following results show both the spectral data gathered by scanning defined surface areas and the elemental composition of remarkable objects obtained by point analysis.

Chemical composition of sandstone. On the basis of existing documentation on the construction of Málaga Cathedral[37] and previous mineralogical and petrographical studies as well as the chemical analysis of major, minor and trace elements,[38] sandstone in the main façade (constructed between 1721 and 1782) has been labeled as an intermediate sandstone consisting of *protoquartzites* and *subarkoses*, which are composed of quartz (70–90% SiO_2), feldspars [$M(Al_xSi_yO_8)$] and dolomite (5–25% [$CaMg(CO_3)_2$]). Fe and Mn are also associated with dolomite in its mineralogical formation.

Fig. 2 depicts a representative single-shot spectrum (the most reproducible one within the spectral series) of the sandstone, a common sedimentary rock that constitutes virtually the entire structure of the Cathedral, as well as a series of chemical maps associated to a 40 cm × 40 cm cornice section. These maps were acquired by scanning the surface with a lateral resolution of 2 cm. The area inspected is located at *ca.* 35 m from the sensor. As observed, standoff LIBS analysis fits neatly with the mineralogical analysis. Intense atomic emissions of Si at 390.6 nm, Al at 396.1 nm, Ca at 396.9 nm, and Mg at 383.8 nm are readily assigned along with faint emissions of Mn at 403.1 nm, Sr at 407.8 nm and Fe at 404.6 nm. Also, information from the maps related to the element distribution profiles of the sandstone surface reinforce the results from the chemical analysis. As seen, along the normal direction to the tested surface, the spatial distribution is virtually identical for the elements found. Nevertheless, although highly correlated, some variability in the intensities is observed. This circumstance derives from the porous nature of the sandstone which exhibits bottleneck-shaped voids of size <4 μm.[39]

Chemical composition of marbles. The composition of significant marble sections of the distinctive medallion located in the front façade was also characterized. Fig. 3 shows a picture of the area inspected. The materials are distinguishable to the naked eye by their different colors (white, black and rose). Marbles are metamorphic rocks whose main minerals are calcite ($CaCO_3$) or dolomite, according to the geological setting of their provenance. Fig. 3 also depicts characteristic LIBS spectra from each marble. As shown, the spectra of the three marbles are dominated by atomic and ionic emissions of Ca, self-reversal in some lines being observed. Small contributions of Al and Ti are also noticed. However, while the spectrum of the

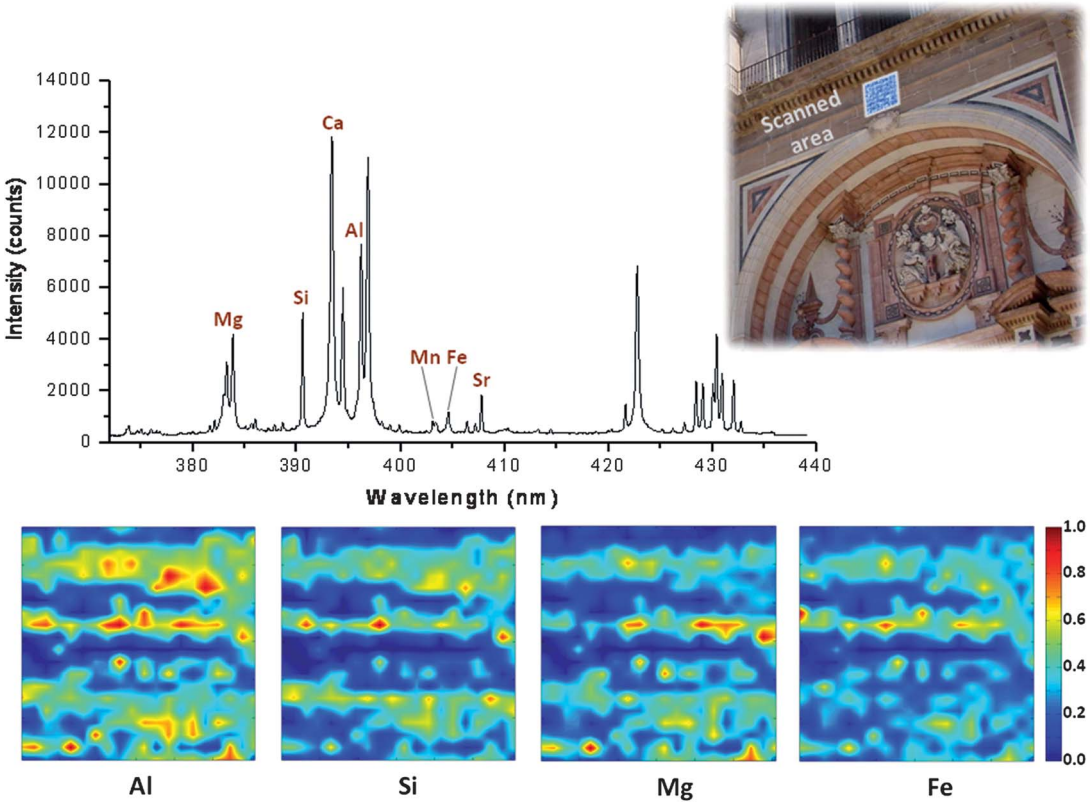

Fig. 2 Representative single-shot standoff LIBS spectrum of sandstone from the cornice upper to the central medallion together with chemical maps related to aluminium, silicon, magnesium and iron distribution profiles. The intensity in each map has been normalized. More details in the body of the text.

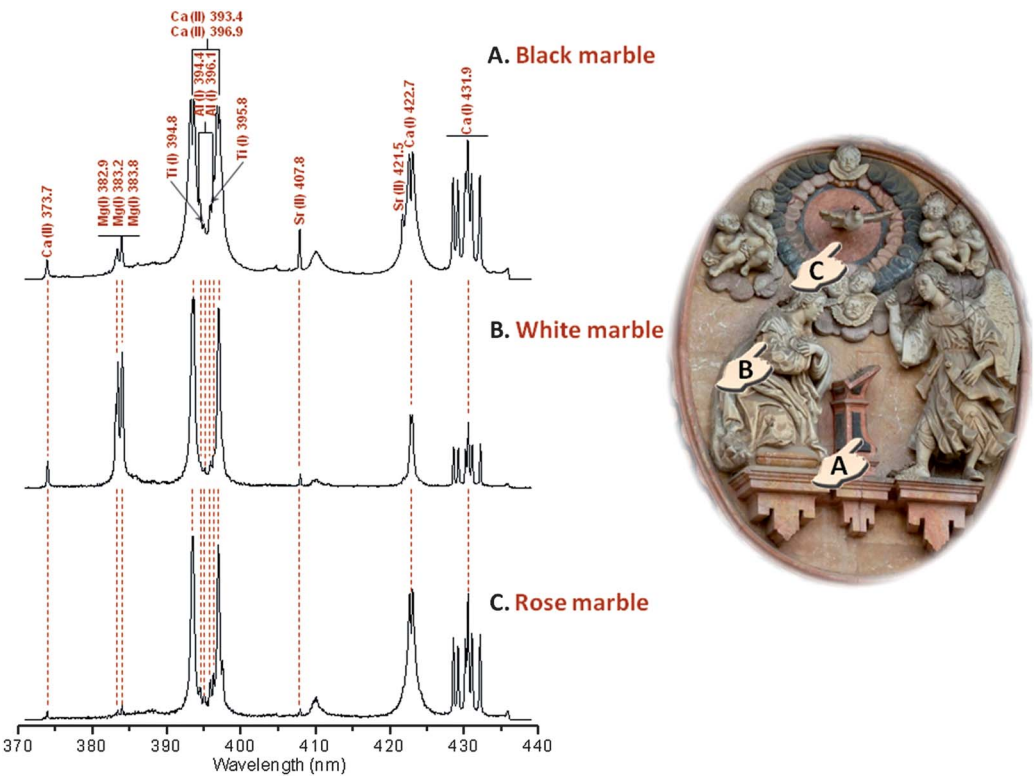

Fig. 3 Characteristic LIBS spectra from the different types of marbles within the main medallion; from top to bottom: black, white and rose.

rose marble (*the background of the dove*) displays mainly Ca lines with very slight contributions of Mg(I) and Sr(II), the spectra of the black and white marbles reveal larger spectral features for these elements. Black marble (*prie-dieu*) exhibits emissions of Sr and Mg of comparable intensity, whereas in the white marble (*statue of the Virgin Mary*) the abundance of Mg is significantly larger than that of Sr.

To check for the consistency of LIBS to discriminate the marble materials, a large set of data acquired on specific positions on the medallion was processed. For this purpose, the ratio of intensities for different elements (Sr(I) at 407.8 nm and Mg(I) at 383.8 nm) to the Ca(I) emission (431.9 nm) was examined. Fig. 4 displays a 3D scatter plot projected onto the subspace of the Sr/Ca and Mg/Ca intensity ratios. Each series of 500 LIBS spectra was gathered from five refreshed sampling points (100 spectra each) within each type of marble. As reflected, the three datasets are grouped in three well-defined clouds. White marble shows Mg/Ca intensity ratios centered near 1.6, whereas the corresponding values for black and rose marbles are close to 0.3. In turn, black and rose marbles differed clearly in their Sr/Ca intensity ratios, ~0.45 and ~0.17, respectively. This sensitivity to carbonate chemistry just discussed demonstrates the capability of standoff LIBS for consistently sorting materials of the same kind. Indeed, the spectral characteristics of the marbles may be used as identity cards for these materials.

It is expected that the quantitative intensities of optical emissions in the marbles of the Málaga district are distinctive enough for identifying the provenance of these different carbonate materials. Hence, based on the spectroscopic information and according to the geology of the quarries of Málaga,[39] it is possible to suggest that the white marble comes from any nearby dolomitic quarries (Monda, Coín, Mijas or Alhaurín de la Torre) whereas black and rose marbles both may originate from Alhaurín el Grande, which is the closer quarry solely supplying calcitic materials.[40]

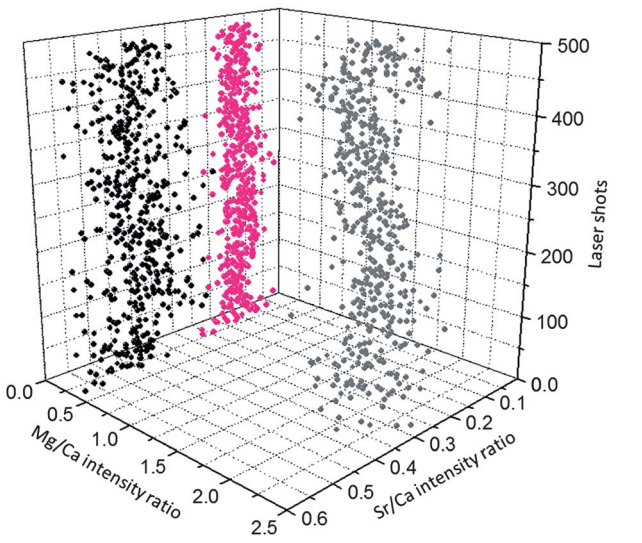

Fig. 4 3D scatter plot projected onto the subspace of the Sr/Ca and Mg/Ca emission intensity ratios for series of 500 single-shot LIBS spectra gathered each from three types of marbles composing the most distinctive medallion and distinguishable by different colorations (white, black and rose).

Standoff LIBS was also used to analyze marbles from different sections of the façade in order to identify their provenance. Three sets of materials, constituted by marble samples of the same color, were examined. Table 1 summarizes the data. As observed, in the same vein, meaningful information again maximized the *inter-class* differences, that is, between marbles of different colors. In contrast, no statistically significant *intra-class* differences were noticed. To recap, the data suggest that the same colored marbles had the same provenance.

Chemical composition of ornamental metallic objects. To close this section, a number of decorative metallic objects located in the façade were analyzed. Fig. 5 depicts the representative standoff LIBS spectra from two metallic ornamental details, namely, the flowers in the vases alongside the medallion and the seals in the corners of the squared frame. As observed, flowers are exclusively constituted by Pb, identified through its characteristic emissions at 405.8 nm. In contrast, the seals were featured by atomic and ionic Cu emissions with small contributions of Pb at 405.8 nm. No significant spectral features apart from mere impurities were eventually identified. These results suggest that the seals are made from the Cu–Pb alloy commonly called *molybdochalkos* (95% Cu/5% Pb) or old Greek metal, a leaded copper bronze often used during the Renaissance.[41] Justification for this seems to lie in the requirements of each ornament. Thus, while a malleable material such as pure Pb was suitable for the elaboration of the flowers, a more rigid material was needed for making the seals.

3.2 Detection of pollutants

Due to its actuation over the course of several hundred years, air pollution severely contaminates and damages the building materials of ancient artifacts. Estimation of both the nature and the amount of pollutants is of crucial importance before advancing in future conservation programs. Phenomena that cause building decay are complex due to the numerous intervening factors. In urban environments, worrisome air pollutants include SO_2, SO_4^{2-}, NO_x, NO_3^-, Cl^-, CO_2, O_3, particulate matter (especially soot from diesel vehicle emissions), and acid rain. On the other hand, the most sensitive materials to pollutants are metals and calcareous stones.[42] With the aim of obtaining quick, *in situ* information on the profiling of contamination, LIBS analysis of the soiling on these materials was also pursued.

Inconspicuous contamination. Fig. 6 compares LIBS spectra acquired for the lead flowers in the vases. The top spectrum corresponds to the first shot on the surface, whereas the bottom spectrum was obtained after 300 shots on a single position. Apart from Pb, the first spectrum reveals the presence of pollutant elements, namely Mg, Fe, Si, Ca, Al, Ti, Mn and Sr. This finding suggests that in addition to the ubiquitous elements mainly due to wind blowing from the nearby coast (Mg, Si, Ca, Al, and Sr), anthropogenic sources (characteristically road traffic in urban areas) are also involved in the contamination (Fe, Ti, and Mn).

Table 1 Ratios of Mg/Ca and Sr/Ca emission intensities corresponding to the different marbles employed in the front façade of Málaga's cathedral

Marble description		Emission intensity ratios			
		Mg/Ca		Sr/Ca	
Color	Location	Mean ± s	RSD (%)	Mean ± s	RSD (%)
Black	A (*decorative border upper the front door*)	0.42 ± 0.07	16	0.41 ± 0.08	19
	B (*elliptical frame of the medallion*)	0.56 ± 0.10	19	0.43 ± 0.09	21
	C (*prie-dieu*)	0.35 ± 0.05	13	0.46 ± 0.07	16
White	A (*decorative border upper the front door*)	1.63 ± 0.33	20	0.13 ± 0.07	56
	B (*carved capital from the Solomonic column*)	1.60 ± 0.23	15	0.16 ± 0.04	24
	C (*statue of the Virgin Mary*)	1.86 ± 0.70	40	0.12 ± 0.04	33
Rose	A (*background of the Dove*)	0.25 ± 0.07	26	0.12 ± 0.04	34
	B (*Solomonic column*)	0.25 ± 0.09	37	0.14 ± 0.03	19
	C (*squared frame of the medallion*)	0.22 ± 0.04	14	0.17 ± 0.03	16

Fig. 7 depicts the depth profile of Cu (406.3 nm) normalized to Ca (431.9 nm) from 500 laser pulses delivered to the metallic seal. As can be seen, while the ratio values remain virtually constant along the first 300 laser shots, a progressive increase in the values is observed for deeper pulses. This increase is the result of surface cleaning when the pollutant content relative to Cu decreases. Additionally, the large number of laser pulses to reach the base material gives an approximate idea of the thickness of the contamination layer. The sudden decrease of the Cu/Ca ratio value is due to the hopping of the laser beam to a fresh position within the contaminated seal (see the discussion below on beam wander effects).

Gross contamination. While pollution can go unnoticed by observations at long distances, deposits are more than evident in some areas of the façade. Indeed, dust deposits tend to accumulate in decorative details with pronounced embossments and complex geometry. That fact is evidenced in Fig. 8 which shows a picture from a Solomonic column made of rose marble. As seen in the twisted column, despite its equivalent temporal exposure to weather, two clearly disparate areas due to the orientation of its sections are distinguished: the downward parts that are seemingly clean, and the upward parts showing dirt crusts. Fig. 8 also shows representative LIBS spectra of each section. As shown, the spectrum corresponding to the '*clean*'

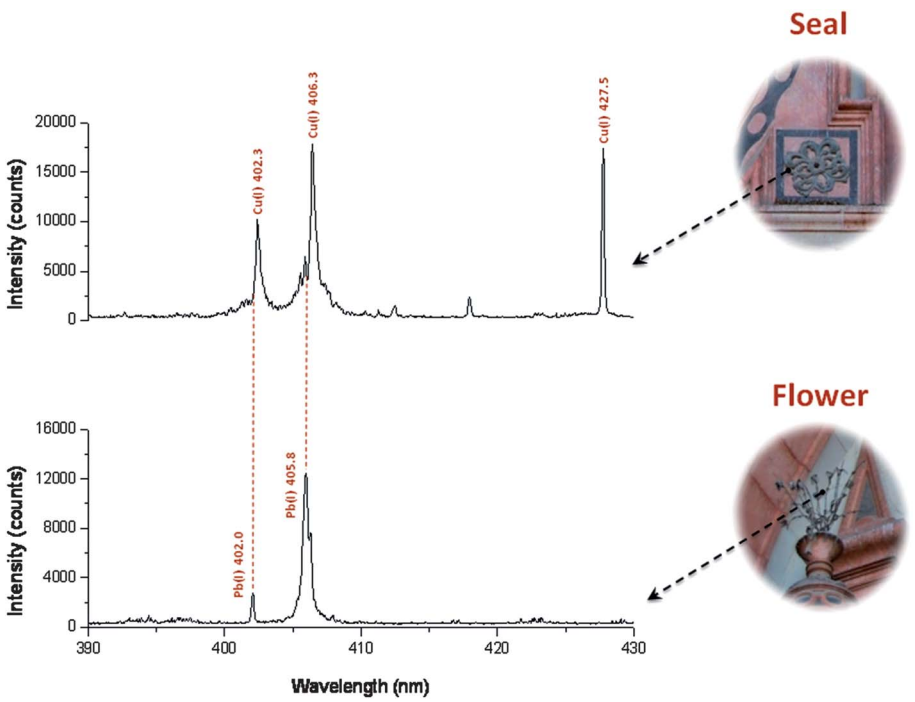

Fig. 5 Representative standoff LIBS spectra of two metallic ornamental elements.

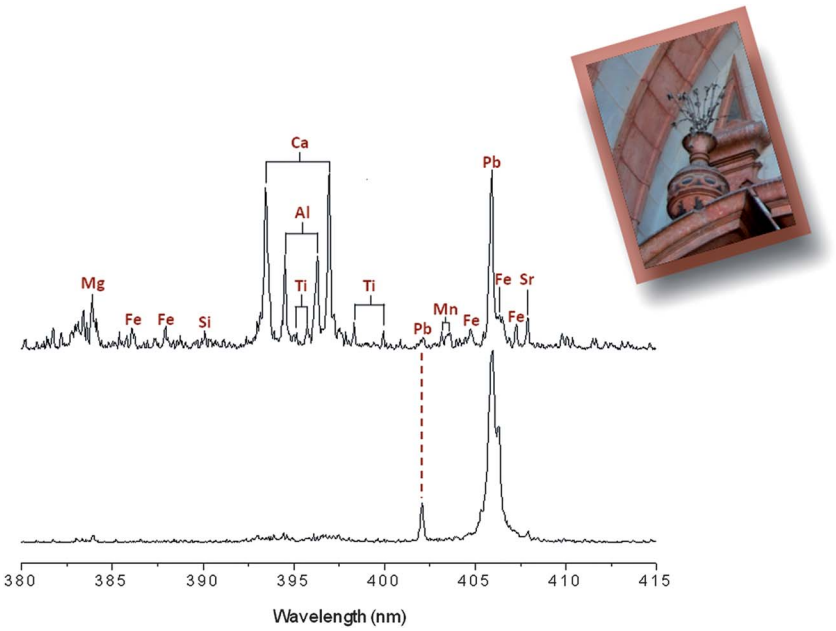

Fig. 6 Comparison between LIBS spectra from polluted and clean cases for the lead flowers in the vases.

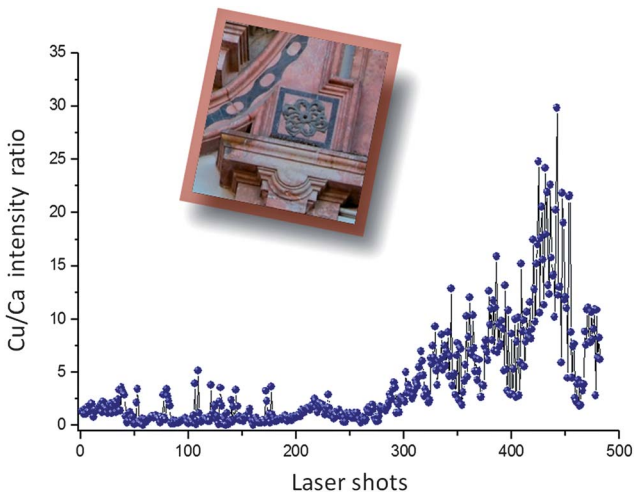

Fig. 7 Evolution profile of the Cu (406.3 nm)/Ca (431.9 nm) intensity ratio from 500 laser pulses in depth on the seal.

surface of the column is characterized by Ca, Al and Ti emissions with small contributions from Mg and Sr, in agreement with the composition of the rose marble studied in the medallion (see Fig. 3). In the spectrum of the '*crust-coated*' surface, apart from Ca, Al and Ti, the intensities of Mg and Sr are much larger than in the clean surface. New lines corresponding to Fe, Si, Mn, Pb and Ba are observed. Table 2 lists the emission wavelengths corresponding to these elements assigned in the standoff LIBS spectrum. Also, the concentrations obtained by inductively coupled plasma optical emission spectrometry (ICP-OES) are quoted. After the crust was carefully removed from the surface, the powdered crust was dissolved through the use of a mixture of $HNO_3/HCl/H_2O_2/HF/H_3BO_3$. Finally, after microwave-assisted acid digestion of the silicate matrix, the total element composition was by ICP-OES under the follow operating conditions: radiofrequency power of 1500 W, nebulizer gas flow of 0.70 L min^{-1}, plasma gas flow of 15 L min^{-1} and auxiliary gas flow of 0.2 L min^{-1}.

As observed, high levels of elements such as Si and Ca, as well as intermediate concentrations of Mg, Fe and Al were detected. These findings may be justified basically with the transport of re-suspended dust or of atmospheric particulate matter from the sea coast located nearby. In the same vein, sources for trace elements such as Ba and Sr may be related to marine aerosols and/or to dust from the Sahara desert, a few hundred kilometers distant from Málaga.[43] Further, trace elements such as Ti, Pb and Mn were detected by standoff LIBS. Hence, anthropogenic factors are not discarded. Soot and metallic particles bearing Pb (major element) as well as Ti and Mn (trace elements) from exhaust emissions of gasoline and diesel engines, respectively, are also considered to trigger the pollution of materials.

In order to better assess the long-term adverse effects of contamination, its *in-depth profile* behavior on marble was examined. This study did not intend to be exhaustive in describing the environmental characteristics of the deposits. Instead, the capabilities of standoff LIBS for describing the behavioral patterns of the pollutants were investigated.

Intensity ratios of several detected elements to the Ca signal (431.9 nm) – the most abundant element in the samples – were considered. Fig. 9 plots the progression profiles of the ratios for series of 500 standoff LIBS spectra gathered from the two surfaces of the Solomonic column. As observed, all datasets are fitted to well-defined profiles for the 'clean' surface. However, while the Al/Ca and Ti/Ca ratios revealed values around 0.5, the remaining ratios showed values close to 0 due to the absence in the parent material of the elements involved. It should be noticed that increased ratio values are recorded in the first few

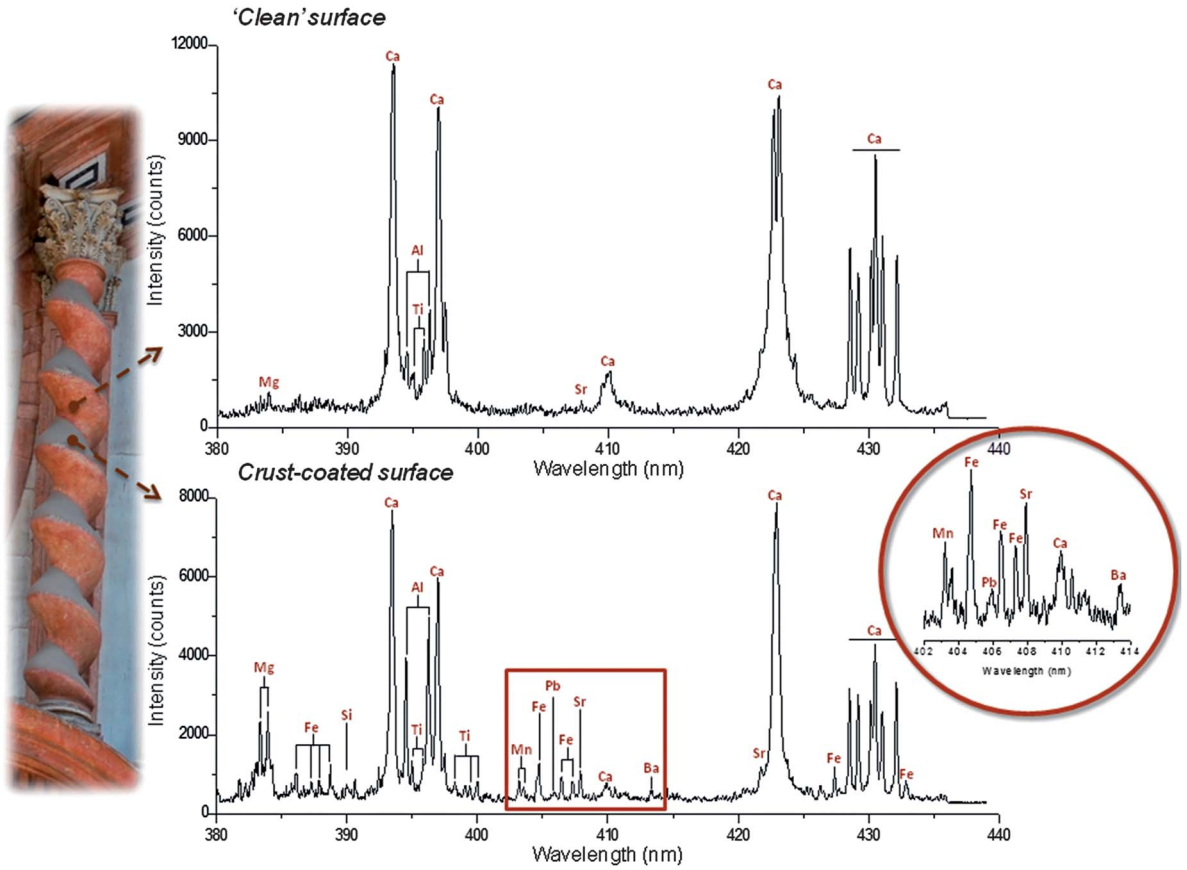

Fig. 8 Spectral comparison between 'clean' and 'crust-coated' sections within the Solomonic column.

shots of all profiles. These initial large ratio values derive from the inconspicuous pollutants present even on the 'clean' surface. The excess ratios are also randomly distributed along the profiles and are due to the sampling of fresh positions. Such an observation is a consequence of the wandering of the beam on the surface caused by wind gusts.[36]

In the 'crust-coated' surface, the depth profiles follow a similar trend, also exhibiting the effects of wind gusts, especially noticeable in the profiles of Si, Fe, Ba, Mn and Pb. However, unlike the discrete variations observed in the clean section of the column, the Al/Ca and Ti/Ca values undergo substantial changes. Aluminium is present in both the mother

Table 2 Emission lines featured in the standoff LIBS spectrum acquired from the soiling that covers the Solomonic column together with the quantitative amount of the detected elements estimated by ICP-OES

		ICP-OES	
Element	Wavelength[a]/nm	Concentration/mg g^{-1}	RSD (%)
Si	390.6	142.0	2.0
Ca	393.4$^{(II)}$, 396.9$^{(II)}$, 422.7, 428.3, 428.9$^{(II)}$, 429.9, 430.3, 430.8, 431.9	135.0	2.0
Mg	382.9, 383.2, 383.8	50.0	3.0
Fe	386.0, 387.9, 388.9, 390.0, 404.6, 406.4, 407.2, 427.2, 432.6	46.0	2.0
Al	394.4, 396.1	33.0	2.0
Ti	394.8, 395.8, 398.2, 399.0, 399.9	2.5	1.0
Pb	402.1, 405.8	0.8	0.5
Ba	413.1	0.8	1.0
Mn	403.1, 403.3, 403.4	0.4	1.0
Sr	407.8$^{(II)}$, 421.5$^{(II)}$	0.2	2.0

[a] Ionic lines have been highlighted with $^{(II)}$.

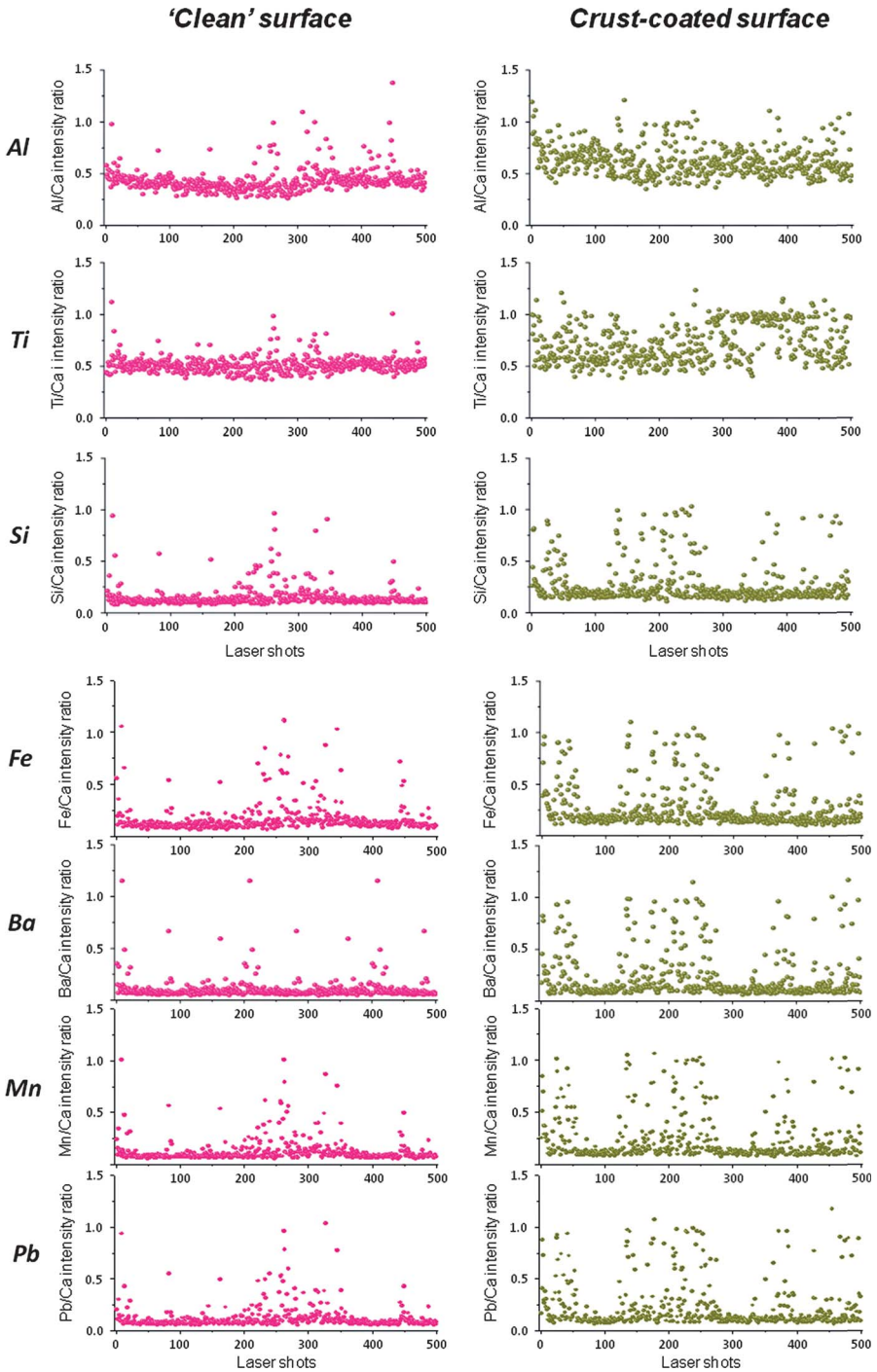

Fig. 9 Evolution profile of intensity of distinct detected elements (from top to bottom: Al, Ti, Si, Fe, Ba, Mn, Pb) to the Ca signal, from 500 laser pulses in depth on 'clean' and 'crust-coated' sections within the Solomonic column.

rock and in the soiled column. This is clearly noticed since the average value of the Al/Ca ratio along the profile (0.63) is almost 70% larger than that observed in the 'clean' surface (0.43). Similar holds true in the case of Ti, passing from 0.52 to 0.72.

Three colored marbles from one of the corners framing the main arc were also assessed. Fig. 10 exhibits a 3D scatter plot projected onto the subspace of the Al/Ca and Ti/Ca emission intensity ratios for series of 500 LIBS spectra gathered from each marble section. As reflected, the three datasets line up in three well-defined clouds. However, although there is similarity between these colored marbles, the values for ratios differ from those obtained in the case of the Solomonic column, thus reflecting that pollution is changing from one area to another. In addition, in the case of the white marble a substantial fall in the values of both ratios is detected after *ca.* 200 laser shots, *i.e.* when the laser drills deeper into the sample. This circumstance is due to the Al and Ti content relative to Ca content being significantly less, suggesting that those two elements may be

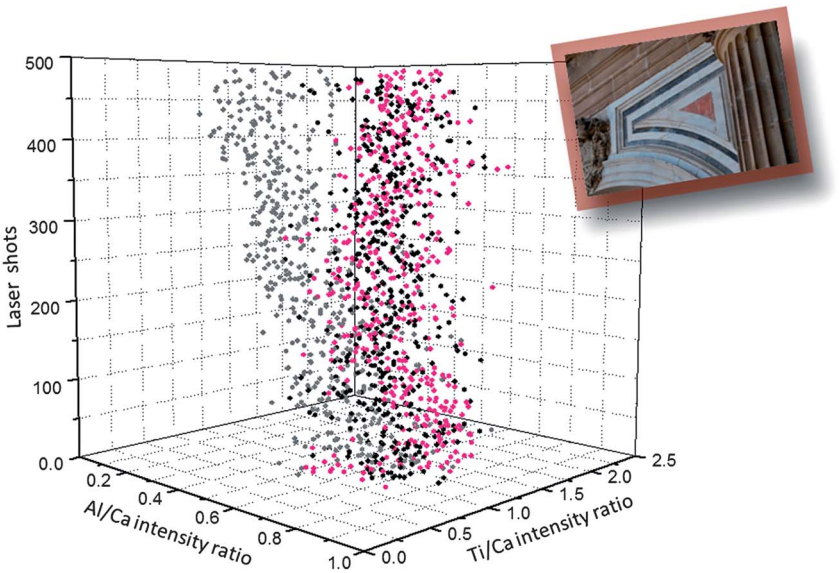

Fig. 10 3D scatter plot projected onto the subspace of the Al/Ca and Ti/Ca emission intensity ratios for series of 500 LIBS spectra gathered from each of the three types of marbles within the corners framing the main arc and distinguishable by different colorations (white, black and rose).

relevant pollutants embedded in the surface of the marbles. Furthermore, this disparity between the trends indicates that the stability of the scabs on the surfaces of the black and rose marbles is higher than on the surface of the white marble. Circumstances that fit perfectly with the more serious effect of sulfation process on calcitic marbles than on dolomitic ones.[44]

4 Conclusions

This work presents, for the first time, the use of LIBS for an *in situ* standoff characterization of the materials forming an historical building and the nature of their cumulative soiling over time. These studies were conducted in the frame of a project aimed at verifying the feasibility of standoff LIBS analysis of unmovable and tangible architectural heritage material. Marbles, sandstone and metals of the ornamental assets in the architectural scenes of the front façade of the Cathedral of Málaga have been described. Further, the LIBS technique has been demonstrated to display high sensitivity to detect the presence of inconspicuous soiling and gross crusts on the surfaces of different ornamental elements. Nevertheless, the possibility to faithfully attribute pollution to either anthropogenic sources or to be influenced by the vicinity of a marine and coastal environment is still an issue. Procurement of all this site-specific information is of primary importance prior to planning restoration programs or taking decisions about whether a close-contact access plan is needed or not. Further studies are underway to confirm these results and uncover the sources and mechanisms of such a contamination.

Several improvements on the sensing platform are under development. A long-range, high-definition imaging subsystem is being installed with the aim of contributing to monitoring the appearance of the treated surface in real-time, the degree of cleaning or any unwanted effect induced by laser irradiation. Results demonstrate that scaffolding of huge dimensions is not necessary for inspection surveys of architectural heritage in so far as there is a line of sight towards the target.

Acknowledgements

This work was supported by Project CTQ11-24433 of the Ministerio de Economia y Competitividad, Secretaría de Estado de Investigación, Desarrollo e Innovación of Spain. The authors wish to thank the Instituto Andaluz de Patrimonio Histórico, Consejería de Cultura y Deporte and Fernando Ramos de Rivas (Quantity Surveyor to the Fabric of Málaga Cathedral), for his kind collaboration in the measurement campaign in the Cathedral of Málaga. I. Gaona thanks the concession of her FPI research contract, through the CTQ2007-60348 Project, to the Spanish Ministerio de Economía y Competitividad, Secretaria de Estado de Investigación, Desarrollo e Innovación.

References

1 O. Hahn, *Anal. Bioanal. Chem.*, 2012, **402**, 1411.
2 B. H. Stuart, *Analytical Techniques in Art Conservation*, John Wiley & Sons, Chichester, 2007.
3 *Non-destructive microanalysis of cultural heritage materials*, ed. K. Janssens and R. Van Grieken, Elsevier, The Netherlands, 2004.
4 G. Vittiglio, S. Bichlmeier, P. Klinger, J. Heckel, W. Fuzhong, L. Vincze, K. Janssens, P. Engstromo, A. Rindby, K. Dietrich, D. Jembrih-Simburger, M. Schreiner, D. Denis, A. Lakdar and A. Lamotte, *Nucl. Instrum. Methods Phys. Res., Sect. B*, 2004, **213**, 693–698.
5 F. J. Fortes, J. Cuñat, L. M. Cabalín and J. J. Laserna, *Appl. Spectrosc.*, 2007, **61**, 558–564.
6 I. Cacciari, D. Ciofini, M. Mascalchi, A. Mencaglia and S. Siano, *Anal. Bioanal. Chem.*, 2012, **402**, 1585–1591.

7 J. Cuñat, F. J. Fortes, L. M. Cabalín, F. Carrasco, M. D. Simón and J. J. Laserna, *Appl. Spectrosc.*, 2008, **62**, 1250–1255.
8 B. Sallé, P. Mauchien and S. Maurice, *Spectrochim. Acta, Part B*, 2007, **62**, 739–768.
9 R. Gaudiuso, M. Dell'Aglio, O. De Pascale, G. S. Senesi and A. De Giacomo, *Sensors*, 2010, **10**, 7434–7468.
10 C. Fotakis, D. Anglos, V. Zafiropulos, S. Georgiou and V. Tornai, *Lasers in the Preservation of Cultural Heritage. Principles and Applications*, Taylor and Francis, Boca Raton, 2007.
11 F. J. Fortes and J. J. Laserna, *Spectrochim. Acta, Part B*, 2010, **65**, 975–990.
12 A. Giakoumaki, K. Melessanaki and D. Anglos, *Anal. Bioanal. Chem.*, 2007, **387**, 749–760.
13 S. Duchêne, V. Detalle, R. Bruder and J. B. Sirven, *Curr. Anal. Chem.*, 2010, **6**, 60–65.
14 L. Caneve, A. Diamanti, F. Grimaldi, G. Palleschi, V. Spizzichino and F. Valentini, *Spectrochim. Acta, Part B*, 2010, **65**, 702–706.
15 E. Xenogiannopoulou, C. Andreouli and C. Stournaras, *J. Nano Res.*, 2009, **8**, 61–70.
16 L. Angeli, C. Arias, G. Cristoforetti, C. Fabbri, S. Legnaioli, V. Palleschi, G. Radi, A. Salvetti and E. Tognoni, *Lasers Chem.*, 2006, **2006**, 1–8.
17 P. Maravelaki-Kalaitzaki, *Anal. Chim. Acta*, 2005, **532**, 187–198.
18 F. J. Fortes, M. Cortés, M. D. Simón, L. M. Cabalín and J. J. Laserna, *Anal. Chim. Acta*, 2005, **554**, 136–143.
19 M. Brai, G. Gennaro, T. Schillaci and L. Tranchina, *Spectrochim. Acta, Part B*, 2009, **64**, 1119–1127.
20 F. Colao, R. Fantoni, P. Ortiz, M. A. Vazquez, J. M. Martín, R. Ortiz and N. Idris, *Spectrochim. Acta, Part B*, 2010, **65**, 688–694.
21 P. Maravelaki-Kalaitzaki, D. Anglos, V. Kilikoglou and V. Zafiropulos, *Spectrochim. Acta, Part B*, 2001, **56**, 887–903.
22 M. P. Mateo, T. Čtvrtníčková, E. Fernández, J. A. Ramos, A. Yáñez and G. Nicolas, *Appl. Surf. Sci.*, 2009, **255**, 5579–5583.
23 F. Colao, R. Fantoni, V. Lazic, A. Morone, A. Santagata and A. Giardini, *Appl. Phys. A: Solids Surf.*, 2004, **79**, 213–219.
24 F. Colao, R. Fantoni, V. Lazic, L. Caneve, A. Giardini and V. Spizzichino, *J. Anal. At. Spectrom.*, 2004, **19**, 502–504.
25 R. Grönlund, M. Lundqvist and S. Svanberg, *Appl. Spectrosc.*, 2006, **60**, 853–859.
26 A. Giakoumaki, I. Osticioli and D. Anglos, *Appl. Phys. A: Mater. Sci. Process.*, 2006, **83**, 537–541.
27 R. Bruder, V. Detalle and C. Coupry, *J. Raman Spectrosc.*, 2007, **38**, 909–915.
28 M. Hoehse, A. Paul, I. Gornushkin and U. Panne, *Anal. Bioanal. Chem.*, 2012, **402**, 1443–1450.
29 M. F. Alberghina, R. Barraco, M. Brai, T. Schillaci and L. Tranchina, *Proc. of SPIE O3A: Optics for Arts, Architecture, and Archaeology II*, ed. L. Pezzati and R. Salimbeni, 2009, vol. 7391, p. 739107.
30 S. Guirado, F. J. Fortes, V. Lazic and J. J. Laserna, *Spectrochim. Acta, Part B*, 2012, **74–75**, 137–143.
31 V. Raimondi, G. Cecchi, D. Lognoli, L. Palombi, R. Grönlund, A. Johansson, S. Svanberg, K. Barup and J. Hällström, *Int. Biodeterior. Biodegrad.*, 2009, **63**, 823–835.
32 P. Weibring, D. Lognoli, R. Chiari, G. Cecchi, H. Edner, T. Johansson, L. Pantani, S. Svanberg, D. Tirelli and M. Trambusti, *Proc. of SPIE Laser Techniques and Systems in Art Conservation*, ed. R. Salimbeni, 2001, vol. 4402, p. 4402.
33 D. Lognoli, G. Lamenti, L. Pantani, D. Tirelli, P. Tiano and L. Tomaselli, *Appl. Opt.*, 2002, **41**, 1780–1787.
34 G. Cecchi, L. Pantani, V. Raimondi, L. Tomaselli, G. Lamenti, P. Tiano and R. Chiari, Fluorescence lidar technique for the remote sensing of stone monuments, *J. Cult. Herit.*, 2000, **1**, 29–36.
35 L. Palombi, D. Lognoli, V. Raimondi, G. Cecchi, J. Hällström, K. Barup, C. Conti, R. Grönlund, A. Johansson and S. Svanberg, *Opt. Express*, 2008, **16**, 6794–6808.
36 J. J. Laserna, R. Fernández Reyes, R. González, L. Tobaria and P. Lucena, *Opt. Express*, 2009, **17**, 10265–10276.
37 A. Llordén, *Historia de la construcción de la catedral de Málaga*, Universidades y Academias, Spain, 1999.
38 E. Galán, M. I. Carretero and E. Mayoral, *Eng. Geol.*, 1999, **54**, 287–298.
39 M. P. Lapuente, B. Turi and P. Blanc, *Appl. Geochem.*, 2000, **15**, 1469–1493.
40 F. Origlia, E. Gliozzo, M. Meccheri, J. E. Spangenberg, I. Turbanti Memmi and E. Papi, *Eur. J. Mineral.*, 2011, **23**, 857–869.
41 B. M. Weisman and C. L. Reedy, *Mater. Res. Soc. Symp. Proc.*, 2002, **712**, DOI: http://dx.doi.org/10.1557/Proc-712-II10.1.
42 J. Watt, J. Tidblad, V. Kucera and R. Hamilton, *The Effects of Air Pollution on Cultural Heritage*, Springer, Berlin, 2009.
43 C. Guieu, M. D. Loyë-Pilot, C. Ridame and C. Thomas, *J. Geophys. Res.*, 2002, **107**, AAC 4–1–AAC 4–12.
44 K. Malaga-Starzec, I. Panas and O. Lindqvist, *Appl. Surf. Sci.*, 2004, **222**, 82–88.

